2018 IEEE/RSJ International Conference on Intelligent Robots and Systems (IROS)
Madrid, Spain, October 1-5, 2018

A New Robot Fly Design That is Easier to Fabricate and Capable of Flight and Ground Locomotion

Yogesh M. Chukewad, Avinash T. Singh, Johannes M. James, and Sawyer B. Fuller

***Abstract*— Efforts to engineer insect-sized (∼100 mg) robots are motivated by their potential advantages relative to larger robots, such as greater deployment numbers at the same cost. Previous iterations have demonstrated controlled flight, but were limited in terms of locomotion capabilities outside of flight. They also consisted of many parts, making them difficult to fabricate. Here we present a re-design that lowers the center of mass, allowing the robot to additionally land without the need for long legs. Furthermore, we show that the new design allows for wing-driven ground locomotion. This is achieved by varying the speed of downstroke relative to the upstroke of the flapping wings, which also allows for steering. By landing and subsequently moving along the ground, the robot can negotiate extremely confined spaces and underneath obstacles, as well as navigate to precise locations for sensing operations. The new design also drastically reduces the number of parts, simplifying fabrication. We describe the new design in detail and present results demonstrating these capabilities, as well as feedback-stabilized flights.**

I. INTRODUCTION

Robots the size of common insects like a honeybee (∼100 mg) have the potential for improved performance relative to larger robots in tasks that benefit from small size or large deployment numbers. Examples include gas leak detection, assisted agriculture, or operation around humans without impact hazard. Historically, a key challenge for robots that small was finding a suitable manufacturing method to create the necessary sub-millimeter articulated structure and actuation systems. Additionally, actuators that are in common use in larger scale robots, such as the electric motors that actuate the propellers in most quad-rotor style drones, do not scale down favorably to insect scale in terms of efficiency or power density [1]. This is because surface area-dependent losses such as coulomb friction and electrical resistance take on a greater importance as scale reduces [2]. Recently, however, a suitable manufacturing process and actuation technology was demonstrated that allowed for controlled flights in an 81 mg robot [3]. This robot was built using a diode-pumped solid-state laser and pin-aligned sheet adhesion to fabricate the necessary components [4], and was actuated by piezo-driven flapping wings that emulated the motion of insects [5]–[8]. The mechanism required to convert the actuator motion to wing motion for generating aerodynamic lift is discussed in [9].

The work in [3] demonstrating controlled flight by an 81 mg robot relied on feedback control of its upright orientation using retro-reflective marker-based motion capture. When upright, its long axis extends vertically as in the left image of Fig. 2, raising its center of mass and making it challenging to achieve a successful landing without toppling over. Successful landings with that design required leg extensions that nearly doubled the vehicle's size [10]. An alternative is to use switchable electrostatic adhesion [11] for perching and takeoffs on vertical or overhanging surfaces, but this adds complexity including a high-voltage source, requires a small amount of additional power to remain attached, and is not required for ground-based landings.

The insect robot design of [3] also suffers from being very difficult to fabricate because it requires hand assembly of a relatively large number of discrete components. It also consists of a number of failure-prone steps. An alternative was proposed in [4] that reduced the number of parts by taking inspiration from children's pop-up books. A robotic

The authors are with the Department of Mechanical Engineering, University of Washington, Seattle, WA 98195 yogeshc@uw.edu

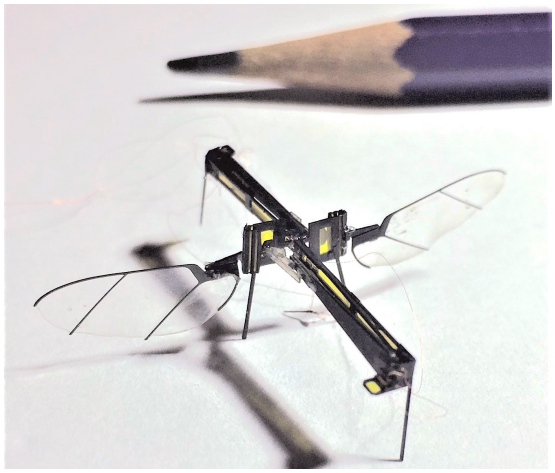

Fig. 1. The redesigned system: University of Washington RoboFly. Each wing measures 13 mm in length and is driven by a separate piezoelectric cantilever actuator. By extending the actuators forward and aft, the center of mass is positioned near the base of the wing pair so that there is no net torque during flight. The entire robot weighs 74 mg. The tip of a standard pencil is shown in the background for scale.

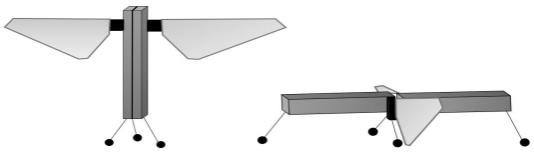

Fig. 2. The U. Washington RoboFly has a low center of mass that allows for a greater diversity of locomotion capability including flight, landing and ground ambulation. (left) In the previous design, a high center of mass precluded landing without long, cumbersome leg extensions. (right) the RoboFly's lowered center of mass removes this limitation.

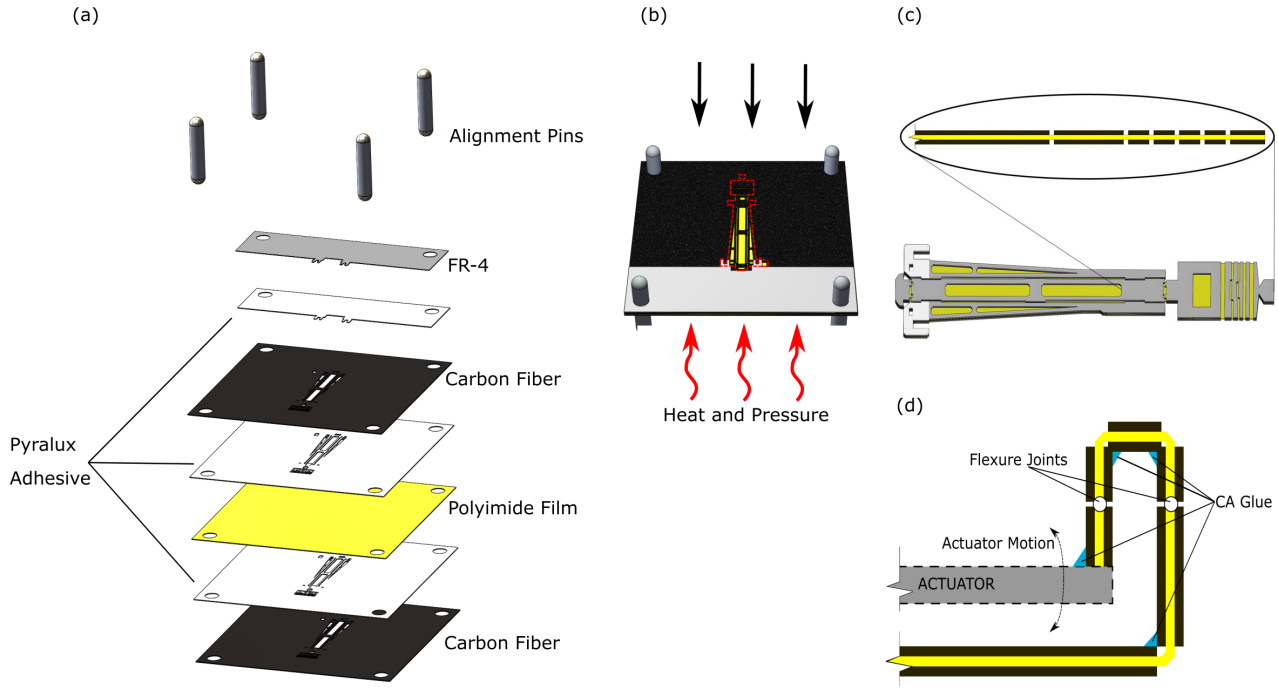

Fig. 3. (a) An exploded view of the layup before curing. (b) Layup during the curing process under predetermined pressure and temperature. (c) Cured laminate after initial release cuts, with magnified sectional view showing the transmission portion. (d) Side view of the folded transmission showing the relative position of the actuator.

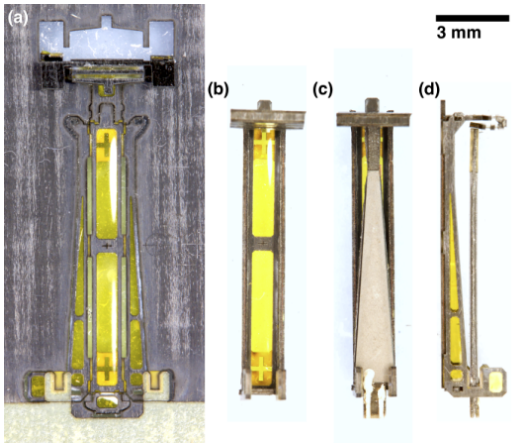

Fig. 4. Folding and actuator insertion post-cure. (a) the laminate in its scaffolding after the transmission component has been folded downward. (b) The scaffolding is cut from the airframe, and the remaining folds are performed. (c) and (d) show two different views of the airframe once an actuator is added.

fly design was demonstrated that consisted of a fabrication step that required actuating a mechanism with only a single degree of freedom. But this design approach is complex, requiring 22 layers with many interdependencies between layers.

This paper describes a new design of an insect-sized flying robot, which we call the University of Washington RoboFly (Fig. 1), that is intended to overcome the deficiencies of previous designs described above.

First, our design has a lower center of gravity. This facilitates landing on the ground, and furthermore we show that it is also possible for the robot to use its wings to push itself along the ground once landed. The difference relative to the previous design [3], [12] is illustrated in Fig. 2. By re-using the wings to power ground locomotion, we are able to avoid the additional complexity and weight of a separate walking mechanism.

Second, our design introduces a fabrication process in which the basic wing actuation unit to be composed of a single laminate, simplifying fabrication relative to earlier designs.

In section II, we introduce the new design and its fabrication. Multi-modal locomotion capabilities that include ground locomotion, takeoff and landing are discussed in section III. Power consumption for the newly developed ground locomotion capability and flight is discussed in section IV.

II. DESIGN AND FABRICATION

Our design re-orients the piezo actuators relative to the transmission, so that they extend horizontally as in Fig. 1. The new orientation of the piezo actuators allows for a much lowered center of gravity without causing pitch or rolling torques.

Our design also simplifies fabrication by combining the airframe, transmission, and actuator attachment hardware into a single laminate sheet. In the previous design that flew [3], these were many separate parts. Combining these into a single laminate reduces the number of discrete parts and

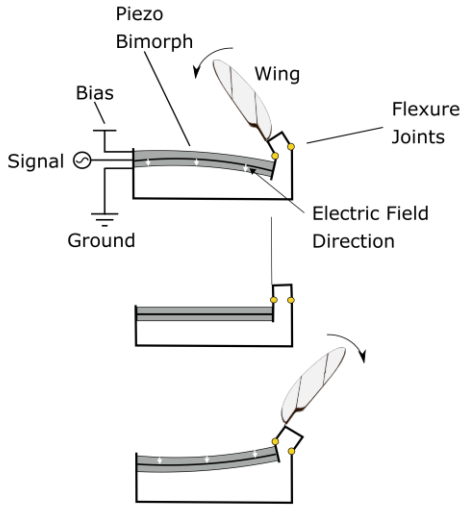

Fig. 5. Diagram of the mechanism of piezoelectric cantilever actuation of the wings. The piezo actuator drives large-amplitude wing motion through small strain changes. The piezo actuator is configured as a bimorph cantilever, consisting of a carbon fiber layer sandwiched between top and bottom piezo sheets. The top surface of the bimorph is charged to a constant high voltage, while the bottom surface is tied to ground per "simultaneous drive" configuration. An alternating signal is connected to the middle layer, providing an alternating electric field in the piezo material. This produces alternating small strains through the reverse piezoelectric effect, which is manifested as motion at the tip of the cantilever. A microfabricated transmission amplifies these tip motions into large ($\sim$ 90 deg) wing motions. This diagram shows the mechanism as seen from above; motion of the wings causes airflow downward, into the page.

facilitates fabrication during prototyping. Many design features and alignment steps can be built into the design of the laminate. For example, the laminate consists of castellated folds [13] that impose a precise rotation axis, and mechanical interlocks that can constrain folds to a specific angle.

The laminate is machined and assembled using the following steps:

1) Two carbon fiber composites are laser machined with different features using a diode-pumped solid-state frequency tripled Nd:Yag laser with 355 nm wavelength (PhotoMachining, Inc.) to create the top and bottom layers.
2) A modified acrylic adhesive (FR1500 Pyralux) is laser cut to match the respective carbon fiber layer features and is then used to bond flexible inner layers of the multilayer design.
3) A layer of 12.5-micron polyimide film (Kapton) is laser cut and is placed between the two adhesive layers.
4) Polished stainless steel pins align these layers and ensure that the features are placed correctly.
5) The layup as shown in Fig. 3(a) is cured in a heat press at predetermined temperatures and pressures: 200°C; ramp up at 1000°C/min; 70 psi as in Fig. 3(b).
6) The layup is placed back in the laser system where it is re-aligned rotationally and in translation relative to the beam. Release cuts are machined as necessary.
7) The transmission is folded and glued with cyanoacrylate adhesive as in Fig. 3(c). The resulting shape can be seen from the side in Fig. 3(d) and from the top in Fig. 4(a).
8) The rest of the body is then laser cut to release from scaffolding as in Fig. 4(b).
9) An actuator is then carefully placed and glued down in the slots provided on the airframe, as shown in Fig. 4(c, d).
10) A wing is glued to a wing hinge, and the assembly is then glued to the transmission. The wing hinge acts as a connector between the transmission and the wing, and allows the angle of attack to change passively [12].
11) Two of these half-fly assemblies are glued together at the middle on a specially-designed mating surface to complete one full RoboFly.
12) 30-micron diameter carbon fiber rods are glued to the static surface of the transmission and at the front and back extremes of the body to form the legs.
13) A wire bundle consisting of four 51-gauge insulated copper wire is then carefully soldered onto the actuators' bases to complete the electronic connections.

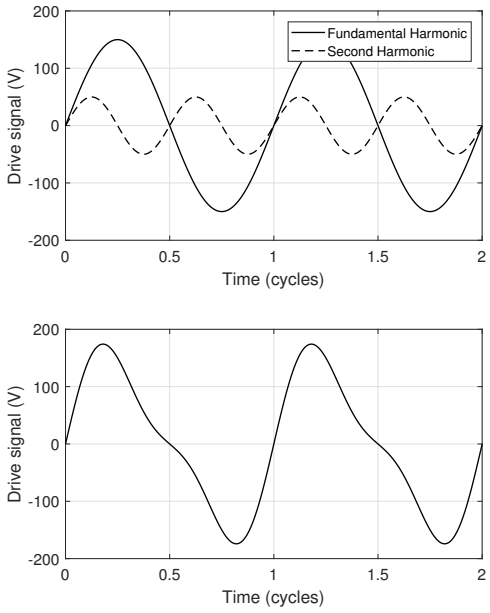

Fig. 6. The addition of a second harmonic signal causes a differential stroke speed. (top) The sinusoidal drive signal to the wings and the second harmonic at 0.3 times the fundamental amplitude. (bottom) The sum of the two signals.

III. MULTI-MODAL LOCOMOTION

The design presented here aims to develop a robot capable of intermittent flights. To do so, the robot must be capable of performing successful takeoffs and landings. In order to achieve the goal, there are three areas of motion that need to be addressed— ground locomotion, takeoff and landing.

A. Ground Locomotion

The RoboFly has a set of four passive legs as shown in Fig. 1. The front and the rear ends have one leg each, and the center section has two legs. This configuration is chosen

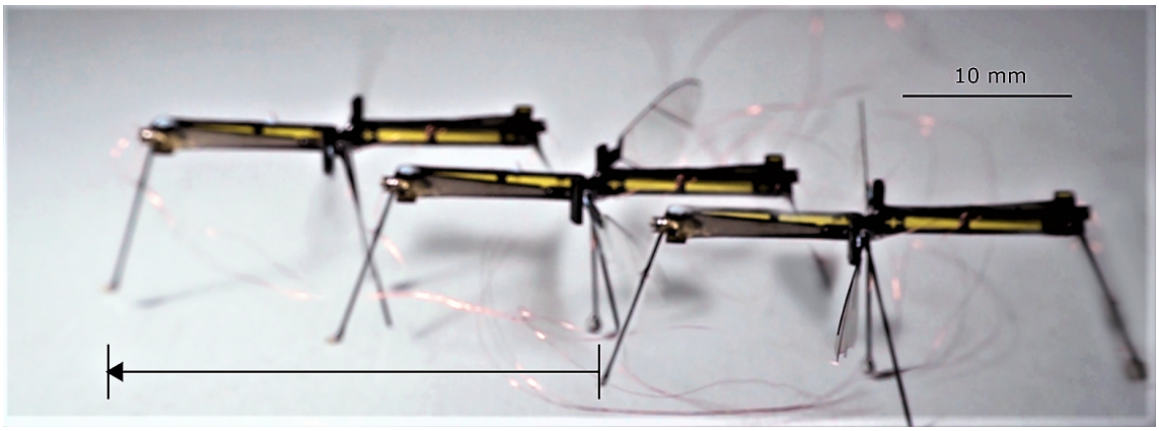

Fig. 7. Without a steering command, the robot moves forward over the ground (progress is denoted by black arrow at bottom)

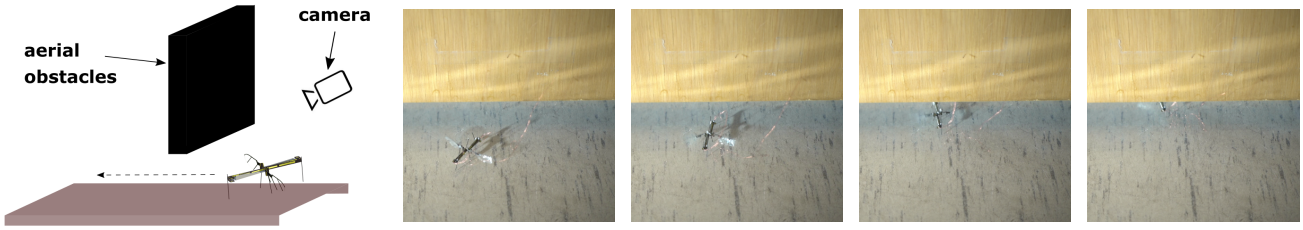

Fig. 8. (left) Ground locomotion allows the robot to navigate under aerial obstacles. (right) The robot is shown ambulating under a closed door, which would not be possible by flying.

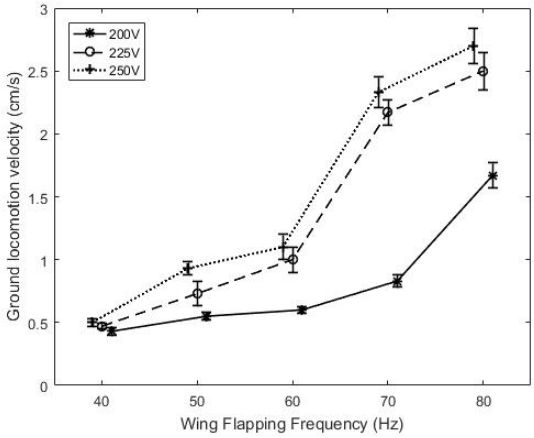

Fig. 9. Ground locomotion velocity increases with increasing signal amplitude and flapping frequency. For comparison, liftoff occurs at approximately 140 Hz.

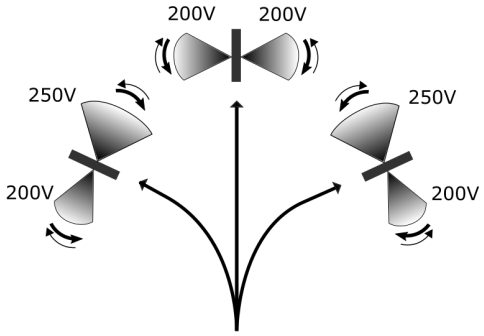

Fig. 10. A top view of ground locomotion and steering. Steering can be performed by driving the wings with unequal signals. Thickness of the arrows corresponds to the stroke speed. Here, the rearward stroke is faster than the forward stroke, causing forward motion.

to balance the need for a stable platform and fabrication simplicity.

Ground locomotion is performed by flapping the wings at a lower frequency than is needed for takeoff. The stroke amplitude remains the same for ground locomotion as flight and is determined by the amplitude of the drive signal voltage as can be visualized in Figs. 5, 6. By adding a second harmonic at double the frequency, so that either the downstroke or upstroke is faster (Fig. 6), the robot is made to move forward or backward. For example, forward motion occurs when the signal to the wings drives them rapidly backwards. A similar mechanism was proposed to induce torques about a vertical or yaw axis in [3].

It was hypothesized that this motion is due to the robot momentarily exceeding coulomb friction during the fast period of the wing stroke. To determine whether this motion was primarily driven by inertial or by aerodynamic forces, an experiment was performed in which the wings were replaced by carbon rods with identical mass and moment of inertia. In these and all subsequent locomotion experiments, the piezo actuators were driven by a desktop computer running Simulink Real-Time (MathWorks, Natick, MA, USA) and amplified using three high voltage amplifiers (Trek 2205, Lockport, New York). One amplifier supplies the DC 'bias'

(a) T=250 ms (b) T=500 ms (c) T=750 ms (d) T=1000 ms (e) T=1250 ms

Fig. 11. The RoboFly turns right by 90°. A pencil tip is shown in the background for scale.

signal to both actuators; the other two amplifiers each supply the separate sinusoidal drive signals to the two wings. When supplied with various different driving signals that moved the robot when it was equipped with wings, it was observed that the robot equipped with carbon rods did not move significantly from its initial position. This indicates that the forces causing the ground locomotion are mainly due to the aerodynamic drag acting on the wings. To understand why this should be so, we note that the Reynolds' number of the wing is approximately 3000 [14], that is, dominated by inertial forces. This indicates that drag is proportional to the square of the wing velocity according to $f_d = \frac{1}{2} C_D \rho A v^2$, where C_D is the aerodynamic drag coefficient, ρ is the air density, A is the frontal area of the wing, and v is the velocity of the wing. Therefore, a faster wingstroke with a higher v will produce higher drag than a slow stroke.

Ground locomotion along a straight line is demonstrated in Fig. 7 and the supplementary video [15]. Photographs at intermediate time instances in the evolution are overlaid using transparency. The wings were flapped at 70 Hz at maximum amplitude (250 V), well below the frequency needed to take flight. Similarly, a ground ambulation that allows the robot to navigate under a closed door is demonstrated in Fig. 8 and the video [15].

To determine how the driving signal affects locomotion, the RoboFly was driven in the forward direction with a range of different voltages and frequencies as shown in Fig. 9. Resulting displacements were measured with a ruler, and the speed was calculated by dividing by the time taken. The results show that robot velocity increases with increasing flapping frequency and amplitude. We conjecture that the large velocity increases that occur at different amplitudes are the result of the robot overcoming coulomb friction at a critical phase of wing flapping. The small increase from 225 V to 250 V is likely attributable to the small resulting additional stroke amplitude.

Steering is performed by varying the signals given to each flapping wing independently. To steer the body to the left, the left wing is flapped at a reduced drive signal amplitude than the right wing, as depicted in Fig. 10. The rate of rotation is determined by the relative drive signal amplitude difference in the two wings. A sharp turn can be achieved by keeping one wing stationary while the other wing flaps. The extreme continuation of this would be the yaw about the vertical axis passing through the center of the body, for which the wings are flapped 180° out of phase. A continuous range of turn angles can be achieved by modulating the difference between left and right wing drive signals.

Fig. 11 and the supplementary video [15] show that the robot is able to steer its motion, in addition to moving forward. Here, the wings were flapped at 70 Hz as above, but the left wing was flapped with larger drive signal amplitude (250 V) whereas the right wing was flapped at a lower value (200 V). Similarly, the robot was made to steer left with these amplitudes reversed, as well as move backwards.

B. Takeoff and Flight

Frames taken from a clip of a controlled takeoff (included in the supplementary video [15]) are presented in Fig. 12. In this video, feedback from a retroreflective marker-based camera motion capture system (Model Prime13, OptiTrack, Inc., Salem, OR) was used to stabilize attitude. Using a model of the robot fly consisting of the predicted thrust from the wings as estimated from its mass, the length of the wings, and estimated moments of inertia, control inputs were abstracted to desired angular accelerations a_x and a_y about its body $x-$ and $y-$ axes, respectively. Roll torque is actuated through differential thrust and pitch torque is actuated by changing the mean stroke angle, as in [3]. Prior to this controlled flight, the robot was hand-trimmed by adding baseline pitch and roll torque commands to overcome any bias that occurred as a result of manufacturing irregularity. This was performed by observing the flight in high-speed video and iteratively applying compensatory torques until the robot flew approximately vertically in open loop. The control law simply added rotational damping, which provided upright stability as in [16]:

$$\begin{aligned} a_x &= k_d \hat{\omega}_x \\ a_y &= k_d \hat{\omega}_y, \end{aligned}$$

where $\hat{\omega}_x$ and $\hat{\omega}_y$ are the x- and y components of the angular velocity vector as estimated by motion capture. Yaw motion was not controlled. The feedback gain k_d was tuned experimentally to balance instability (caused by latency in the feedback loop) against the need to maximize damping. A value of -30 was found to give good results. The wings were flapped at 140 Hz with a 250 V amplitude (peak-to-peak). The RoboFly can be seen taking off without any significant change in pitch and roll orientations. The altitude in this case is approximately 5 cm.

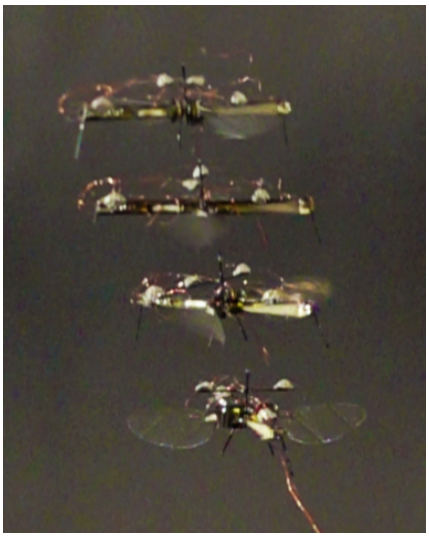

Fig. 12. A short flight in which the robot is kept upright by controlling roll and pitch orientations with the help of feedback from a motion capture arena. The robot is subject to a small yaw bias torque that caused it to rotate leftward in this video. Frames are captured at 50 ms intervals.

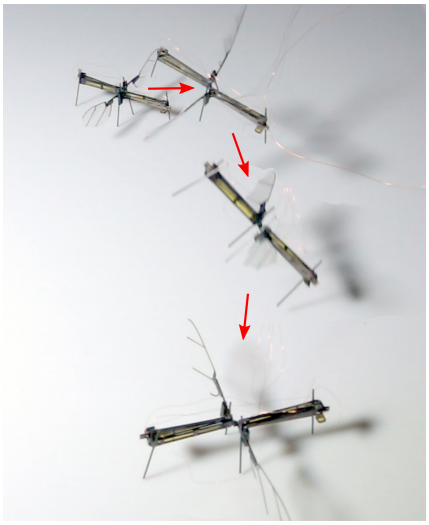

Fig. 13. A demonstration of open-loop takeoff and landing

C. Landing

The third objective of this work is to achieve successful landing, which must be robust and repeatable in order to achieve intermittent flights. This is facilitated by our robot's low center of mass (Fig. 2). Lowered center of mass helps in preventing the robot body from toppling. We were able to achieve multiple successful landings under open loop control as demonstrated in Fig. 13 and the supplementary video [15]. For these flights, as above, the wings were flapped at 140 Hz and 250 V drive signal amplitude. To demonstrate robustness of landing, the robot was flown in open loop, so that it did not always land level. In future work, we expect that a feedback-stabilized robot that remains level, as was demonstrated in the takeoff flight shown in Fig. 12, will allow for repeatable landings. Once landed on the ground, the robot is positioned to easily undertake the next desired locomotion task.

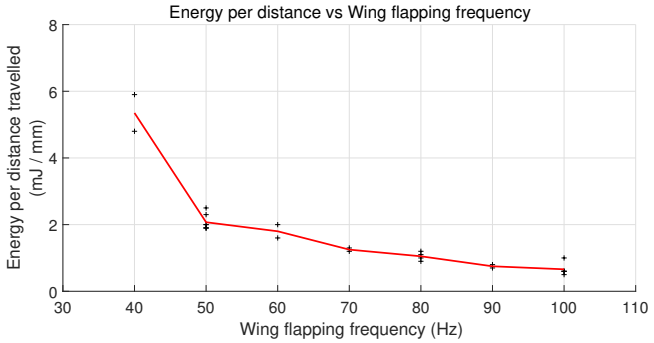

Fig. 14. The cost of transport (*COT*), the energy expended per unit distance traveled, decreases with increasing drive frequency f.

IV. POWER CONSUMPTION

The voltage and current to the bimorph actuators was measured at a sampling frequency of 10 kHz, from the current measurement port of the amplifiers. The instantaneous power was time averaged over an integer number of wing strokes in order to compute the average power consumption of the robot. In order to estimate power requirements as they would be for an onboard driver circuit implementation such as demonstrated in [17] which does not utilize the energy recovery mechanisms discussed in [18], reverse power from the center node of the bimorph actuator is zeroed in this work. This modeling assumption reflects the realistic reality that during the part of the wing stroke in which the sinusoidal drive signal voltage is decreasing, positive charge leaving the center node of the actuator (in the conventional current sense) must be dumped to ground and cannot be recovered to the high voltage bias rail.

Eq. 1 shows the computation of the cost of transport (*COT*), that is, the energy used per unit distance traveled. The measured power was integrated over time and divided by the estimated distance traveled by the robot as measured by the motion capture system.

$$COT = \frac{\int V I_r \, \mathrm{d}t}{S} \tag{1}$$

Where S is the 3D distance traveled, V is the driving voltage, and I is the measured current.

In these experiments, the driving amplitude was 250 V. The results show that the cost of transport decreases with increasing flapping frequency (Fig. 14). This is conjectured to be the result of two competing factors: 1) Electrical input power increases proportionally with driving frequency f because the actuators are principally a capacitive load with current $I \propto C\frac{\mathrm{d}V}{\mathrm{d}t}$. 2) The aerodynamic lift increases with f^2 for the same reason that drag does (Section III). Therefore, as frequency increases, the robot is expected to spend proportionally less of its time in physical contact with the surface, reducing friction losses. Together these factors suggest a dependence of *COT* on frequency, as observed.

Measurements also indicated that the trend of decreasing *COT* with increasing frequency continued when the robot was in flight. The *COT* was measured in flights traversing 0.2 m as measured by motion capture while flapping at

140 Hz. The *COT* for flying locomotion was ~ 0.02 mJ/mm, which is $\sim 25\times$ less than the most efficient ambulation.

V. FUTURE WORK

Leg design can be improved by minimizing friction and by the addition of shock absorption to improve the resilience of the robot. Minimizing friction would improve the over-ground *COT* discussed in Section IV, and reduce disturbances while moving over irregular terrain.

Alternative locomotion modes such as jumping should be evaluated. Hopping locomotion can be quite efficient due to advantageous scaling effects as robot size and weight are reduced [19], although additional weight and complicated hopping mechanisms are ill suited to honeybee-sized flying robots as discussed in Section III. Fei in [20] demonstrates bio-inspired jumping mechanisms and discusses the dynamics and optimization.

Ground locomotion may be improved by adopting a different control signal architecture at low-frequency. This work uses a 2-component Fourier basis to cause differential stroke speed and achieve the ground locomotion as shown in Fig. 6, but the attainable difference in speed between upstroke and downstroke is limited as frequency decreases. A higher-order approximation would not have this limitation because a waveform similar to a 'sawtooth' (but still smooth so as to not damage the actuator) would allow reducing the frequency f while still executing a very fast wing stroke in one direction.

It is also important to investigate the underlying mechanisms of the ground locomotion demonstrated here. Although inertial dynamics of the flapping motion were experimentally determined to be less significant than the aerodynamic drag acting on the wings (Section III), there is still uncertainty as to the role of vibratory mechanisms in the ground locomotion. If vibratory mechanism is significant, then the feet could be redesigned to exploit this; e.g. directional spines could serve to selectively favor a direction of motion.

VI. CONCLUSIONS

This paper presents a new design with two major contributions to the field of insect-sized robotics. It simplifies fabrication, and allows the robot to perform landing and ground locomotion in addition to flight without cumbersome leg extensions.

In the new design, the airframe and transmission are all folded from a single laminate sheet. Compared to previous work, the design presented here represents an intermediate solution that lies between the many parts of [3], [12] and the single laminate sheet composed of many layers of [13] (Table I). We believe this represents a valuable intermediate between these two extremes because on the one hand our design with two laminates gains many of the benefits of pop-up book manufacturing, such as having few parts and the ability to precision align small components. And on the other hand, it does not inherit the substantial complexity imposed by large number of interdependencies among layers. This reduces the difficulty of design iteration. Furthermore, we believe our intermediate approach is still amenable to automated manufacturing, by assuming that some steps will be performed by small robotic end-effectors.

	Ma [3]	**Sreetharan [13]**	**This work**
# Layers:	5	22	**7**
# Distinct Parts:	14	1	**8**

TABLE I. Comparison of number of layers and discrete parts required in different construction methods for creating insect-sized flying robots. Our design balances layer number and complexity and parts count to facilitate more rapid design evolution and prototyping while retaining the superior alignment characteristics of the multilayer designs. (Legs for support are not counted.)

We showed that the lowered center of gravity of the robot allows it to land and ambulate along the ground including steering, in addition to flight. The cost of transport was found to be substantially higher than that of free-flight, so this mode of locomotion is better suited to precise motions, such as to precisely position a sensor. We additionally showed that ground ambulation can allow our robot to reach new places that are not accessible through flight, such as moving under a typical door. This represents a capability to negotiate an obstacle that heretofore exclusively the domain of the most adept ground robots, and impossible with air robots.

Our robot's multi-modal locomotion capabilities resemble those of larger robots. For example, [21] developed a larger bio-inspired robot (393 g, 72 cm) capable gliding flight as well as the ability to ambulate by rotating its ailerons. [22] developed a bio-inspired micro-vehicle (100 g, 30.5 cm) capable of performing aerial locomotion using wings and terrestrial locomotion using whegs. Similarly, [23] developed a bipedal ornithopter (11.4 g, 28 cm) with flapping wings for aerial locomotion and rotary legs for terrestrial locomotion. A 30 g robot took an approach similar to our robot by using the four propellers of its flight apparatus to steer its motion. These were used to steer a simple walking mechanism that was capable of moving in only one direction [24]. To our knowledge this work represents the first example of multi-modal locomotion capability at insect scale.

The capability of landing will allow the robot to perform intermittent flights. This will be useful for providing power to the robot. For example, the robot could more easily collect power from a laser because the laser would not have to follow it [17], [25], [26], or from magnetic resonance coupling, as has previously been demonstrated on a ground robot in [27]. Furthermore, landing will be necessary for the robot to collect energy from ambient energy sources such as indoor light or radio frequency signals such as WiFi [28] or cellular. In the case of energy harvesting from aeroelastic flutter [29], ground locomotion may be needed to position the robot in the flow. While these sources tend to be very minute and therefore insufficient to power larger robots, they may be enough to power the UW RoboFly for a reasonable fraction of the time, if it can land and charge between flights. The horizontal design of this work facilitates the attachment of power electronics [17] and sensors such as ultralight cameras [30].

REFERENCES

[1] R. J. Wood, B. Finio, M. Karpelson, K. Ma, N. O. Pérez-Arancibia, P. S. Sreetharan, H. Tanaka, and J. P. Whitney, "Progress on picoair vehicles," *The International Journal of Robotics Research*, vol. 31, no. 11, pp. 1292–1302, 2012.

[2] W. S. Trimmer, "Microrobots and micromechanical systems," *Sensors and actuators*, vol. 19, no. 3, pp. 267–287, 1989.

[3] K. Y. Ma, P. Chirarattananon, S. B. Fuller, and R. J. Wood, "Controlled flight of a biologically inspired, insect-scale robot," *Science*, vol. 340, no. 6132, pp. 603–607, 2013.

[4] J. P. Whitney, P. S. Sreetharan, K. Y. Ma, and R. J. Wood, "Pop-up book mems," *Journal of Micromechanics and Microengineering*, vol. 21, no. 11, p. 115021, 2011.

[5] P. Chirarattananon and R. J. Wood, "Identification of flight aerodynamics for flapping-wing microrobots," in *Robotics and Automation (ICRA), 2013 IEEE International Conference on*. IEEE, 2013, pp. 1389–1396.

[6] M. H. Dickinson and K. G. Gotz, "Unsteady aerodynamic performance of model wings at low reynolds numbers," *Journal of Experimental Biology*, vol. 174, no. 1, pp. 45–64, 1993.

[7] M. H. Dickinson, F.-O. Lehmann, and S. P. Sane, "Wing rotation and the aerodynamic basis of insect flight," *Science*, vol. 284, no. 5422, pp. 1954–1960, 1999.

[8] C. P. Ellington, "The aerodynamics of hovering insect flight. vi. lift and power requirements," *Phil. Trans. R. Soc. Lond. B*, vol. 305, no. 1122, pp. 145–181, 1984.

[9] Z. A. Khan and S. K. Agrawal, "Design of flapping mechanisms based on transverse bending phenomena in insects," in *Robotics and Automation, 2006. ICRA 2006. Proceedings 2006 IEEE International Conference on*. IEEE, 2006, pp. 2323–2328.

[10] P. Chirarattananon, K. Y. Ma, and R. J. Wood, "Adaptive control for takeoff, hovering, and landing of a robotic fly," in *Intelligent Robots and Systems (IROS), 2013 IEEE/RSJ International Conference on*. IEEE, 2013, pp. 3808–3815.

[11] M. Graule, P. Chirarattananon, S. Fuller, N. Jafferis, K. Ma, M. Spenko, R. Kornbluh, and R. Wood, "Perching and takeoff of a robotic insect on overhangs using switchable electrostatic adhesion," *Science*, vol. 352, no. 6288, pp. 978–982, 2016.

[12] K. Y. Ma, S. M. Felton, and R. J. Wood, "Design, fabrication, and modeling of the split actuator microrobotic bee," in *Intelligent Robots and Systems (IROS), 2012 IEEE/RSJ International Conference on*. IEEE, 2012, pp. 1133–1140.

[13] P. S. Sreetharan, J. P. Whitney, M. D. Strauss, and R. J. Wood, "Monolithic fabrication of millimeter-scale machines," *Journal of Micromechanics and Microengineering*, vol. 22, no. 5, p. 055027, 2012.

[14] R. J. Wood, "The first takeoff of a biologically inspired at-scale robotic insect," *IEEE transactions on robotics*, vol. 24, no. 2, pp. 341–347, 2008.

[15] "Autonomous Insect Robotics Laboratory, University of Washington," Available: http://depts.washington.edu/airlab/IROS2018-1906.html, 2018.

[16] S. B. Fuller, M. Karpelson, A. Censi, K. Y. Ma, and R. J. Wood, "Controlling free flight of a robotic fly using an onboard vision sensor inspired by insect ocelli," *Journal of The Royal Society Interface*, vol. 11, no. 97, p. 20140281, 2014.

[17] J. James, V. Iyer, Y. Chukewad, S. Gollakota, and S. B. Fuller, "Liftoff of a 190 mg laser-powered aerial vehicle: The lightest wireless robot to fly," in *Robotics and Automation (ICRA), 2018 IEEE International Conference on*. IEEE, 2018.

[18] M. Karpelson, G.-Y. Wei, and R. J. Wood, "Driving high voltage piezoelectric actuators in microrobotic applications," *Sensors and actuators A: Physical*, vol. 176, pp. 78–89, 2012.

[19] R. M. Alexander, *Principles of animal locomotion*. Princeton University Press, 2003.

[20] F. Li, W. Liu, X. Fu, G. Bonsignori, U. Scarfogliero, C. Stefanini, and P. Dario, "Jumping like an insect: Design and dynamic optimization of a jumping mini robot based on bio-mimetic inspiration," *Mechatronics*, vol. 22, no. 2, pp. 167–176, 2012.

[21] L. Daler, S. Mintchev, C. Stefanini, and D. Floreano, "A bioinspired multi-modal flying and walking robot," *Bioinspiration & biomimetics*, vol. 10, no. 1, p. 016005, 2015.

[22] R. J. Bachmann, F. J. Boria, R. Vaidyanathan, P. G. Ifju, and R. D. Quinn, "A biologically inspired micro-vehicle capable of aerial and terrestrial locomotion," *Mechanism and Machine Theory*, vol. 44, no. 3, pp. 513–526, 2009.

[23] K. Peterson and R. S. Fearing, "Experimental dynamics of wing assisted running for a bipedal ornithopter," in *Intelligent Robots and Systems (IROS), 2011 IEEE/RSJ International Conference on*. IEEE, 2011, pp. 5080–5086.

[24] Y. Mulgaonkar, B. Araki, J.-s. Koh, L. Guerrero-Bonilla, D. M. Aukes, A. Makineni, M. T. Tolley, D. Rus, R. J. Wood, and V. Kumar, "The flying monkey: a mesoscale robot that can run, fly, and grasp," in *Robotics and Automation (ICRA), 2016 IEEE International Conference on*. IEEE, 2016, pp. 4672–4679.

[25] V. Iyer, E. Bayati, R. Nandakumar, A. Majumdar, and S. Gollakota, "Charging a smartphone across a room using lasers," *Proceedings of the ACM on Interactive, Mobile, Wearable and Ubiquitous Technologies*, vol. 1, no. 4, p. 143, 2018.

[26] T. J. Nugent and J. T. Kare, "Laser power beaming for defense and security applications," in *Unmanned systems technology XIII*, vol. 8045. International Society for Optics and Photonics, 2011, p. 804514.

[27] M. Karpelson, B. H. Waters, B. Goldberg, B. Mahoney, O. Ozcan, A. Baisch, P.-M. Meyitang, J. R. Smith, and R. J. Wood, "A wirelessly powered, biologically inspired ambulatory microrobot," in *Robotics and Automation (ICRA), 2014 IEEE International Conference on*. IEEE, 2014, pp. 2384–2391.

[28] V. Talla, B. Kellogg, B. Ransford, S. Naderiparizi, S. Gollakota, and J. R. Smith, "Powering the next billion devices with wi-fi," in *Proceedings of the 11th ACM Conference on Emerging Networking Experiments and Technologies*. ACM, 2015, p. 4.

[29] M. Bryant, E. Wolff, and E. Garcia, "Aeroelastic flutter energy harvester design: the sensitivity of the driving instability to system parameters," *Smart Materials and Structures*, vol. 20, no. 12, p. 125017, 2011.

[30] S. Balasubramanian, Y. Chukewad, J. James, B. Geoffrey, and S. B. Fuller, "An insect-sized robot that uses a custom-built onboard camera and a neural network to classify and respond to visual input," in *Biomedical Robotics and Biomechatronics (BioRob), 2018 IEEE RAS/EMBS International Conference on*. IEEE, 2018.